

## Thermodynamic Phase Transition in Magnetic Reconnection

J. Jara-Almonte<sup>1</sup> and H. Ji<sup>1</sup>

*Princeton Plasma Physics Laboratory, Princeton, New Jersey 08543, USA*

 (Received 1 March 2021; revised 30 April 2021; accepted 17 June 2021; published 29 July 2021)

By examining the entropy production in fully kinetic simulations of collisional plasmas, it is shown that the transition from collisional Sweet-Parker reconnection to collisionless Hall reconnection may be viewed as a thermodynamic phase transition. The phase transition occurs when the reconnection electric field satisfies  $E = E_D \sqrt{m_e/m_i}$ , where  $m_e/m_i$  is the electron-to-ion mass ratio and  $E_D$  is the Dreicer electric field. This condition applies for all  $m_i/m_e$ , including  $m_i/m_e = 1$ , where the Hall regime vanishes and a direct phase transition from the collisional to the kinetic regime occurs. In the limit  $m_e/m_i \rightarrow 0$ , this condition is equivalent to there being a critical electron temperature  $T_e \approx m_i \Omega_i^2 \delta^2$ , where  $\Omega_i$  is the ion cyclotron frequency and  $\delta$  is the current sheet half-thickness. The heat capacity of the current sheet changes discontinuously across the phase transition, and a critical power law is identified in an effective heat capacity. A model for the time-dependent evolution of an isolated current sheet in the collisional regime is derived.

DOI: [10.1103/PhysRevLett.127.055102](https://doi.org/10.1103/PhysRevLett.127.055102)

Magnetic reconnection is a fundamental plasma process responsible for rapidly releasing stored magnetic energy and changing the magnetic topology. Reconnection occurs in nearly all magnetized plasma environments: from highly collisional to nearly collisionless kinetic systems. A wide variety of physical effects and instabilities influence the reconnection process, such as the Hall effect [1], electron kinetic effects [2,3], and plasmoid instabilities [4–6]: many of which were empirically organized into a reconnection phase diagram in analog with a thermodynamic phase diagram [7].

Although the reconnection phase diagram is a successful tool for organizing parameter space, the question of whether there truly exist phase transitions between different regimes has not been rigorously addressed. In reconnection, the simplest and most well-established regimes are the slow, collisional [8–11] and fast, collisionless regimes [1,12,13] with a single two-dimensional  $X$  line. This Letter focuses solely on the fundamental physics of the transition between these two regimes.

Previous results for antiparallel reconnection have suggested that the transition occurs when  $\delta = d_i$ , where  $\delta$  is the current sheet half-thickness,  $d_i \equiv c/\omega_{pi}$  is the ion inertial length, and  $\omega_{pi}$  is the ion plasma frequency [14,15]. The importance of  $d_i$  was suggested based on a scaling analysis of the generalized Ohm's law [16]; the presence of fast, dispersive waves [17]; and abundant empirical evidence that  $d_i$  is a relevant length scale within the collisionless regime [18]. However, there is no fully self-consistent first-principles theory that describes the transition or justifies the exact equality  $\delta = d_i$ .

To date, the most comprehensive model of the transition is the catastrophe model of Cassak *et al.* [14], who

examined it in an isothermal two-fluid system. An evolution equation for the current sheet was developed and a bifurcation from the collisional to the Hall regimes was identified [19]. This model has hysteresis, and it was argued that phase diagrams must therefore include history effects [20]. Hysteresis was observed in a two-fluid simulation by artificially modifying the resistivity [14], as well as in a Hall-magnetohydrodynamics (MHD) simulation due to the self-consistent interplay between plasmoid instability and Hall physics [21]. To the authors' knowledge, similar effects have not been observed in fully kinetic simulations, suggesting that the underlying physics of the transition may differ from simplified fluid models. Within kinetic simulations, the transition has been observed in both two and three dimensions, as well as for both electron-positron and electron-ion plasmas [22–25]; and the dynamic thinning of Sweet-Parker current sheets due the Ohmic heating is known to be an important effect [24].

Here, these earlier results are extended by examining fully kinetic particle-in-cell (PIC) simulations that self-consistently evolve from an initial collisional equilibrium, through a Hall regime where electrons and ions are decoupled but classical resistivity is the dominant nonideal effect, and finally into a collisionless, kinetic regime. The evolution of the entropy is examined, and a thermodynamic phase transition is shown to exist between the collisional and Hall regimes. For finite  $m_i/m_e$ , electron gyroviscosity cannot be neglected; and the phase transition occurs when the normalized reconnection electric field satisfies  $\tilde{E} \equiv E \sqrt{m_i/m_e}/E_D = 1$ , where  $E_D = m_e v_{the} \nu_{ei}/e$  is the Dreicer electric field,  $v_{the}$  is the electron thermal speed, and  $\nu_{ei}$  is the electron-ion collision frequency. This condition applies for all  $m_i/m_e$ , including  $m_i/m_e = 1$ , where the Hall

regime vanishes and a direct phase transition from the collisional to the kinetic regime occurs. In the limit  $m_e/m_i \rightarrow 0$ , and assuming a Sweet-Parker equilibrium, this condition reduces to  $\rho_s/\delta = \beta_e/2 \approx 1$ , where  $\rho_s = \Omega_i^{-1} \sqrt{T_e/m_i}$  is the ion sound radius,  $\Omega_i$  is the ion cyclotron frequency, and  $\beta_e = 8\pi n_e T_e/B^2$  is the ratio of the electron pressure to the magnetic field pressure. This condition may also be written as  $\hat{T} \equiv T_e/m_i \Omega_i^2 \delta^2 \approx 1$ .

To further understand the phase transition, both the current sheet heat capacity  $C$  and an effective heat capacity  $\hat{C}$  are introduced.  $C$  is discontinuous across the phase transition corresponding to a change from isobaric to isochoric heating, whereas  $\hat{C}$  obeys a critical power law. These results allow the time-dependent heating model of Stanier *et al.* [24] to be extended into the “nonlinear” regime where the phase transition occurs. It is shown that in idealized and closed systems, Sweet-Parker current sheets will always collapse down to kinetic scales, provided there is enough free magnetic energy; and the collapse timescale only weakly depends on the initial current sheet thickness.

The PIC code vPIC [26,27], along with a Coulomb collision algorithm [22,28], is used to simulate reconnection in a resistive current sheet. The initial setup is a one-dimensional Harris equilibrium with  $\mathbf{B} = B_0 \tanh(x/\delta_0)\hat{z}$ ,  $n_e = n_i = n_b + n_0 \text{sech}^2(x/\delta_0)$ , and  $T_i = T_e = m_i v_{A0}^2/4$ , where  $n_b/n_0 = 0.3$ ,  $\delta_0 = 2d_{i0}$ ,  $d_{i0}^2 \equiv m_i c^2/4\pi n_0 e^2$ , and  $v_{A0}^2 = B_0^2/4\pi(m_i + m_e)n_0$ . An initial long-wavelength perturbation is applied to seed reconnection. For the case discussed in detail,  $m_i/m_e = 40$ ,  $\omega_{pe,0}/\Omega_{e0} = 2$ , and  $\nu_{ei,0}/\Omega_{e0} \approx 0.042$ , corresponding to an initial Lundquist number of  $S_0 = 4\pi L_0 v_{A,up}/\eta_0 c^2 \approx 2200$ , where  $\eta_0$  is the initial Spitzer resistivity,  $v_{A,up}^2 = (n_0/n_b)v_{A0}^2$ , and  $L_0 = L_z/2$ . The domain spans  $L_x \times L_z = 50 \times 100d_{i0}$  and contains  $790 \times 1560$  cells and  $2.5 \times 10^9$  macroparticles. Periodic boundary conditions are used along  $z$ , whereas particle reflecting and electrically conducting boundaries are used along  $x$ . The time dependence of the reconnection rate ( $R = cE_y/Bv_A$ ) and  $\delta/d_i$  are shown in Fig. 1 along with the out-of-plane current density at three representative times corresponding to the collisional, Hall, and kinetic regimes.

Thermodynamic phase transitions often involve change in the entropy or in properties derived from entropy, and several previous studies have examined entropy in PIC simulations [29–32]. The differential (Boltzmann-Gibbs) entropy for a species  $s$  is given by

$$H_s(t) \equiv \int d^3x h_s(\mathbf{x}, t), \quad h_s(\mathbf{x}, t) \equiv - \int d^3v f_s \ln f_s, \quad (1)$$

where  $f_s$  is the single-particle distribution function for species  $s$ . Previous studies have used a plug-in integral estimator where  $h_s$  is integrated over a phase-space histogram [30,32]. For the similar plug-in redistribution estimator, histograms are either slowly converging or

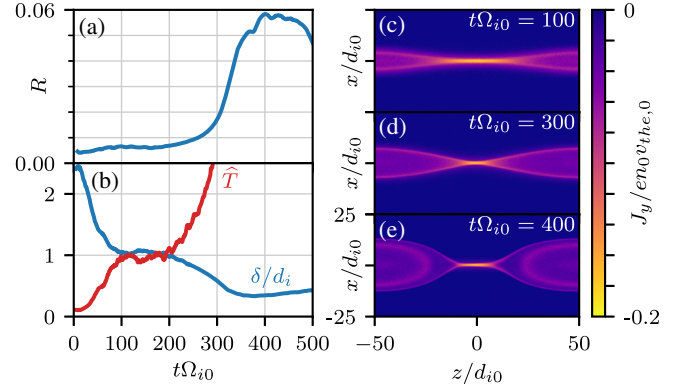


FIG. 1. (a) Reconnection rate and (b)  $\delta/d_i$  and  $\hat{T}$  as a function of time. (c)–(e) Examples of out-of-plane current densities in the (c) collisional, (d) Hall, and (e) kinetic regimes.

inconsistent with significant bias [33], leading to non-negligible systematic error. Here,  $h_s$  is instead computed with the Kozachenko-Leonenko (KL) estimator [34],

$$h_s(\mathbf{x}, t) = -wn[b(k) - b(n)] + w \sum_{i=1}^n \ln \left( \frac{4\pi\rho_{i,k}^3}{3kw} \right), \quad (2)$$

where  $\rho_{i,k}$  is the distance in velocity space from macroparticle  $i$  to its  $k$ th nearest neighbor; and  $b(x) = \psi(x) - \ln x$ , where  $\psi(x)$  is the digamma function. The sum extends over all  $n$  macroparticles in a given cell: each of which has an identical statistical weight  $w$ . The standard choice of  $k = 1$  is used here. The KL estimator is consistent and converges as  $n^{-1/2}$  if  $f$  satisfies regularity conditions [35]. The KL estimator is compared with a histogram estimator in the Supplemental Material [36].

The time evolution of  $H_s$  is shown in Fig. 2(a). Entropy monotonically increases in time and at a rate larger than the numerical entropy gain in an equivalent collisionless case. To the lowest order, entropy is equally partitioned between species since deviations from quasineutrality ( $n_e = n_i$ ) and local thermal equilibrium ( $T_e = T_i$ ) are small. To gain insight into the various regimes of reconnection, the data can be reorganized using the current sheet width rather than time as an independent coordinate; see Figs. 2(b) and 2(c). Two measures are shown,  $d_i/\delta$ , where  $\delta$  is the half width at half maximum of  $J_y$ , and  $d_i$  is evaluated using the  $X$ -point density, and  $\hat{T} \equiv T_e/m_i \Omega_i^2 \delta^2$ , where  $T_e$  is evaluated at the  $X$  point and  $B$  at  $1\delta$  upstream. The former is motivated by significant heuristic and empirical evidence that  $d_i$  is involved in the transition physics, whereas the latter is a dimensionless temperature measure. In these simulations,  $\hat{T}$  predominantly changes due to current sheet thinning and may be equivalently viewed as a measure of  $\delta$ .

An abrupt increase in  $H_s$  can be seen at  $\delta \approx d_i \approx \rho_s$ . This discontinuity in entropy could be interpreted as a first-order thermodynamic phase transition where the net change in entropy across the phase transition is due to a latent heat.

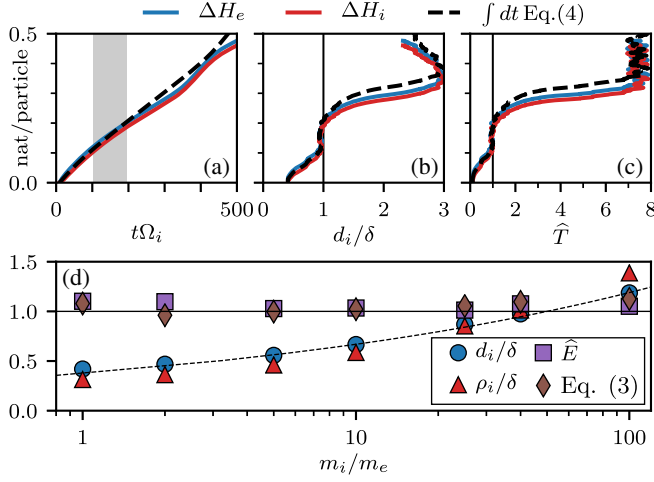


FIG. 2. (a)–(c) Evolution of electron and ion differential entropies,  $H_e$  and  $H_i$ , relative to their initial values (a) as a function of time, and reorganized by (b)  $\delta/d_i$  and (c)  $\hat{T}$  (nat is a dimensionless unit of information). Identified phase transition is shaded in Fig. 2(a) and shown with a vertical line in Figs. 2(b) and 2(c). (d) Quantitative evaluation of proposed transition criteria at time of collisional to Hall (kinetic for  $m_i/m_e = 1$ ) phase transition. Dotted line shows reference  $(m_i/m_e)^{1/4}$  scaling.

However, the phase transition requires a finite time of  $100 \Omega_{i0}^{-1} \lesssim t \lesssim 200 \Omega_{i0}^{-1}$  in order to occur. During this time, ongoing reconnection leads to a continuous production of entropy unrelated to the phase transition itself. As will be shown below, the phase transition appears to be continuous.

By finding the local minimum in  $|d(d_i/\delta)/dH_i|$ , the point at which the collisional to Hall (kinetic for  $m_i/m_e = 1$ ) phase transition occurs can be accurately determined. Various proposed transition criteria are shown as a function of  $m_i/m_e$  and at the time of the phase transition in Fig. 2(d). The criteria of  $\delta = d_i$  and  $\delta = \rho_i$  do not hold for all mass ratios. Rather, it is empirically found that the local criteria of  $\hat{E} \equiv E\sqrt{m_i/m_e}/E_D = 1$  offers an accurate prediction of when the phase transition will occur across all  $m_i/m_e$ . This criterion was previously suggested as an equivalent condition to  $\delta = \rho_s$  since, for large  $m_i/m_e$ , it can be written as  $\rho_s/\delta_{SP} = \beta_e/2$  or  $\hat{T} = (\beta_e/2)^2$ , where  $\delta_{SP} = L/\sqrt{S}$  and  $L$  and  $S$  are the time-dependent half-length and Lundquist number of the current sheet [44].

For finite  $m_i/m_e$ , however,  $\hat{E}$  differs from the large  $m_i/m_e$  limit due to electron gyroviscosity, which is present even in the collisional regime. Within the current sheet, the electron pressure tensor  $\mathbf{P}_e$  has finite off-diagonal elements  $P_{e,xy}$  and  $P_{e,yz}$  due to electron motion in the sheared magnetic field [37]. In the steady-state collisionless limit,  $\partial P_{e,xy}/\partial x \approx \partial P_{e,yz}/\partial z$ , resulting in an electric field of  $E_{NG} \equiv \sqrt{2}(m_e/e)v_{the}dv_{ez}/dz$  [38]. However, these simulations are in a semicollisional regime where  $L \gtrsim v_{the}/\nu_{ei} \gg \delta$ . As a result, collisions suppress  $P_{e,yz}$  but do not affect  $P_{e,xy}$ , and the electric field is reduced by half from the collisionless limit  $(\nabla \cdot \mathbf{P}_e)_y/en \approx E_{NG}/2$ .

This effect is discussed further in the Supplemental Material [36]. Setting  $dv_{ez}/dz = v_A/L$  gives  $E_{NG}/2E_D = d_e^2/\sqrt{2}\delta_{SP}^2$  and the condition

$$\sqrt{\frac{m_i}{m_e}} \frac{\eta J_y + \frac{1}{2} E_{NG}}{E_D} = \frac{2}{\beta_e} \left( \frac{\rho_s}{\delta} + \sqrt{\frac{m_e}{2m_i}} \frac{\rho_s^2}{\delta_{SP}^2} \right) = 1, \quad (3)$$

where  $\delta \neq \delta_{SP}$  in general. For  $m_i/m_e \rightarrow \infty$ , the Sweet-Parker limit is recovered; whereas for  $m_i/m_e \rightarrow 1$ ,  $\rho_s/\delta_{SP} \sim (m_i/m_e)^{1/4}$ . Equation (3) is evaluated and shown to hold within 12% in Fig. 2(d). Although this correction vanishes in the large  $m_i/m_e$  limit, it provides insight into the underlying physics; the local electric field is responsible for the phase transition, and not the current sheet geometry. The remainder of this Letter assumes  $m_i/m_e \gg 1$  and  $n_b/n_0 \ll 1$ , which allow the simpler condition of  $\hat{T} \approx 1$  to be used; up to factors of  $\beta_e \sim 1$ , this is equivalent to the slow-to-fast transition criteria by Cassak *et al.* [14].

In the collisional regime, the rate of entropy production can be estimated as  $dH/dt = (1/T)dQ/dt$ , where  $Q$  is the total heat generated by collisions. Locally, the heat generation is predominantly resistive dissipation  $\eta J^2$ , and so  $dH/dt \approx (4L\delta L_y)(\eta J^2/T) \approx 2N_{SP}\beta^{-1}\nu_{ie}(d_i/\delta)^2$ , where  $\nu_{ie}$  is the ion-electron collision frequency,  $N_{SP} \equiv 4L\delta L_y n$  is the number of particles in the current sheet, and  $L_y$  is the out-of-plane extent. Assuming that  $L$  and  $B$  are constant and using the Spitzer resistivity scaling,  $\eta \sim T^{-3/2}$  gives the scaling  $S \sim n^{-1/2}T^{3/2} \sim \beta^{3/2}n^{-2}$ . For Sweet-Parker current sheets, it then follows that  $N_{SP} \sim n\delta^2 S^{1/2} \sim \beta^{3/4}\delta^2$ . Using subscript 0 to denote initial condition values and taking  $\beta \approx 1$  lead to the estimate

$$\frac{dH}{dt} \approx 2N_{SP,0} \left( \frac{\delta_{SP,0}}{\delta_0} \right)^2 \left( \frac{T_0}{T} \right)^{3/2} \tau_{A0}^{-1}, \quad (4)$$

where  $\tau_A \equiv L/v_A$  is the Alfvén transit time.

Using the  $X$ -line temperature and assuming  $H_e \approx H_i$ , Eq. (4) is integrated to produce the black dashed lines in Figs. 2(a)–2(c), which agree well with the simulation during the collisional phase of  $t \lesssim 100 \Omega_{i0}^{-1}$ . In the collisionless regimes, resistive production of entropy is reduced, and viscous heating and thermal mixing are additional sources of entropy production; these effects will be detailed further in a future paper.

To characterize the phase transition, the viscous electric fields at the  $X$  point ( $\phi_e$  and  $\phi_i$ ) are proposed as phenomenological order parameters,

$$\phi_s = - \left\langle \frac{c(\nabla \cdot \mathbf{P}_s)_y}{q_s n_s B_0 V_{A,0}} \right\rangle, \quad (5)$$

where  $\langle \cdot \rangle$  denotes a local spatiotemporal average in order to reduce statistical noise. These order parameters are shown as a function of  $\hat{T}$  in Fig. 3(a). They are equivalent until the onset of kinetic effects ( $\hat{T} \sim 6$ ), which follows from the

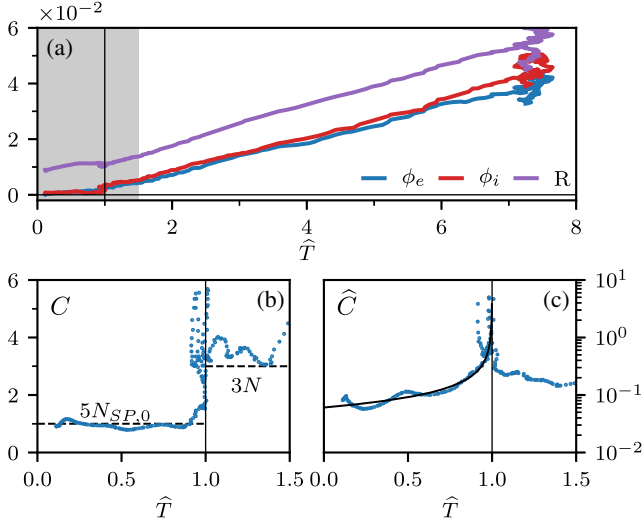


FIG. 3. (a) Order parameters, and (b) and (c) effective heat capacities for the phase transition phase transition as a function of  $\hat{T}$ . Vertical lines mark the phase transition ( $\hat{T} = 1$ ). Shading in Fig. 3(a) shows the region examined in Figs. 3(b) and 3(c), dashed lines in Fig. 3(b) show different limits as discussed in text, and black line in Fig. 3(c) is a power law fit with critical exponent  $\bar{\alpha} = -3/5$ .

momentum equations since  $\nabla \cdot (\mathbf{P}_e + \mathbf{P}_i) = 0$  at a symmetric steady-state  $X$  point. There is an onset at  $\hat{T} = 1$  corresponding to a transition from a disordered phase ( $\hat{T} < 1$ ) to an ordered phase ( $\hat{T} > 1$ ).

The heat capacity of a system changes across a thermodynamic phase transition. Here, two heat capacities are introduced,  $C \equiv TdH/dT$  and  $\hat{C} \equiv \hat{T}dH/d\hat{T}$ , where  $T$  is the  $X$ -point temperature and  $H = H_e + H_i$ .  $C$  and  $\hat{C}$  are shown in Figs. 3(b) and 3(c).  $C$  has a discontinuous change at  $\hat{T} = 1$ , which is consistent with a continuous phase transition.  $\hat{C}$  is asymmetric and diverges at  $\hat{T} = 1$ . For  $\hat{T} < 1$ , there is a critical power law of  $\hat{C} \sim \alpha_0(1 - \hat{T})^{\bar{\alpha}}$  with the best fit scaling exponent  $\bar{\alpha} = -3/5$ .

The two limits for  $C$  can be understood. If there is efficient thermal transport across flux surfaces, then changing the  $X$ -point temperature requires heating the entire plasma volume. This is an isochoric process due to the fixed simulation volume; and  $C \approx 3N$ , where  $N = \int d^3x n$  is the total number of (real) particles per species. A factor of 2 has been included to account for both species. This limit is consistent with the ordered side. In the opposite limit, heat is confined within the current sheet and outflow. This is an isobaric process since the reconnecting magnetic field maintains a constant pressure within the current sheet and  $C \approx 5(N_{SP} + N_{out})$ , where  $N_{out}$  is the number of particles in the outflow. Since the initial equilibrium is a 1D current sheet,  $N_{out,0} = 0$ ; and neglecting the contribution from inflowing particles gives  $N_{SP,0} = N_{SP} + N_{out}$  and  $C \approx C_0 \equiv 5N_{SP,0}$ . This limit is consistent with the disordered side of Fig. 3(b).

As an example of the utility of  $C$  and  $\hat{C}$ , a model for the evolution of a resistive current sheet can be developed. Writing Eq. (4) as  $dH/dt = H'_0 T^{-3/2}$  and using the definition of  $C$  and  $\hat{C}$  give

$$\frac{d\hat{T}}{dt} = \frac{H'_0}{\alpha_0} \frac{\hat{T}}{(1 - \hat{T})^{\bar{\alpha}}} T^{-3/2} \quad (6)$$

$$\frac{dT}{dt} = \frac{H'_0}{C_0} T^{-1/2}. \quad (7)$$

The solution to these equations is

$$T = \left( \frac{3H'_0}{2C_0} t + T_0^{3/2} \right)^{2/3} \quad (8)$$

$$\hat{T} = F^{-1} \left( \frac{C_0}{\alpha_0} \ln \frac{T}{T_0} \right), \quad (9)$$

where

$$F(x) = \int_{\hat{T}_0}^x t^{-1} (1 - t)^{\bar{\alpha}} dt.$$

Collectively, these equations describe Ohmic heating and a collapse of the current sheet, but they differ from previous results that assumed  $T - T_0 \sim t$  and did not include a critical power law [24]. Setting  $\hat{T} = 1$  in Eq. (9) and using Eqs. (8) and (4) lead to an estimate for the collapse timescale of

$$\frac{\tau}{\tau_{A,0}} = \frac{5}{3} (e^{\gamma F(1)} - 1) \left( \frac{\delta_0}{\delta_{SP,0}} \right)^2, \quad (10)$$

where  $\gamma \equiv 3\alpha_0/2C_0$ . For initially thick current sheets,  $\hat{T}_0 \ll 1$  and  $e^{\gamma F(1)} \approx (e^{1/\bar{\alpha}\hat{T}_0})^{-\gamma}$ . In these simulations,  $\gamma \approx 1/11$  and, assuming this is universal,  $\tau \sim 10\tau_{A,0}$  for Sweet-Parker current sheets that are initially  $10^4\rho_s$  thick; whereas for  $\delta \lesssim 5\rho_s$ ,  $\tau \lesssim \tau_{A,0}$ . This model is in good agreement with the simulation data, as shown in Fig. 4; however, further study on the parameter and boundary condition dependence of  $\gamma$  is required before applying these predictions to other systems.

Although derived here in terms of  $\hat{T}$ , an entirely equivalent analysis can be done in terms of  $\hat{E}$ . For the simulations studied, an approximate power law of  $\hat{E}dH/d\hat{E} \approx 0.13C_0(1 - \hat{E})^{-1/2}$  is found. The resulting model agrees well across all values of  $m_i/m_e$  tested, representative examples of which are shown in Fig. 4(c).

In the isothermal limit of  $C \rightarrow \infty$ , this model is identical to the slow-to-fast transition in the catastrophe model of Cassak *et al.* [14], where the Sweet-Parker current sheet is stable. This work extends the catastrophe model by including thermodynamic feedback that results in an instability of the Sweet-Parker current sheet wherein

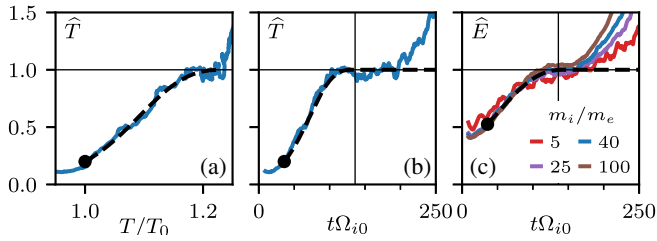


FIG. 4. Comparison with resistive evolution model,  $\hat{T}$  as a function of (a)  $T$  and (b) time, as well as (c)  $\hat{E}$  as a function of time for several values of  $m_i/m_e$ . Solid lines are simulation data, dashed lines are evaluated model predictions, and model initial conditions are shown with a circle. For Figs. 4(a) and 4(b), measured values  $\gamma = 1/11$  and  $\bar{\alpha} = -3/5$  are used, with  $C_0 = 5N_{\text{SP},0}$  calculated from simulation initial conditions and  $H'_0$  evaluated from Eq. (4). In Fig. 4(c), model is developed based on approximate power law quoted in text. Vertical lines in Figs. 4(b) and 4(c) show time estimated from Eq. (10).

Ohmic heating and thinning naturally drive the system toward collisionless regimes. This study does not address whether hysteresis is present in kinetic descriptions, and this remains an open question.

Here, a closed system with a single isolated current sheet was examined; however, in nature, current sheets do not occur in isolation. Additional thermodynamic effects such as thermal transport between the current sheet and the external environment or thermal coupling to neutrals [25] can modify these results. Furthermore, macroscopic physics can be more influential than local current sheet physics in determining current sheet stability and the long-term reconnection rate [45,46], whereas microscopic kinetic physics can strongly influence stability in nearly collisionless systems.

Finally, in large collisional systems, fast reconnection is thought to be driven by the plasmoid instability [4,6,22], resulting in a fractal plasmoid chain that ends at either a Sweet-Parker or a kinetic current sheet [7]. Previous estimates for the division between these two endpoints do not include the resistive evolution described here, which will drive the terminating current sheet toward kinetic scales. Similarly, systems with initial Lundquist numbers below the critical value for plasmoid instability ( $\sim 10^4$ ) can become plasmoid unstable due to self-consistent heating [5,24]. Even without this modification, plasmoid instability itself is regarded as a separate reconnection phase, and future work will investigate whether it may be similarly understood as a phase transition and whether critical behavior is present.

The data that support the findings of this study are openly available in the Princeton University DataSpace [47].

The authors gratefully acknowledge funding from both the General Plasma Science Program from the U.S. Department of Energy's (DOE's) Office of Fusion

Energy Sciences and the Max Planck Princeton Center for Plasma Physics under DOE Contract No. DE-AC02-09CH11466. The simulations presented in this Letter were performed on computational resources managed and supported by Princeton Research Computing, which is a consortium of groups including the Princeton Institute for Computational Science and Engineering and the Office of Information Technology's High Performance Computing Center and Visualization Laboratory at Princeton University.

- [1] J. Birn, J. Drake, M. Shay, B. Rogers, R. Denton, M. Hesse, M. Kuznetsova, Z. Ma, A. Bhattacharjee, A. Otto *et al.*, Geospace environmental modeling (GEM) magnetic reconnection challenge, *J. Geophys. Res.* **106**, 3715 (2001).
- [2] H. J. Cai, D. Q. Ding, and L. C. Lee, Momentum transport near a magnetic X line in collisionless reconnection, *J. Geophys. Res.* **99**, 35 (1994).
- [3] W. Daughton, J. Scudder, and H. Karimabadi, Fully kinetic simulations of undriven magnetic reconnection with open boundary conditions, *Phys. Plasmas* **13**, 072101 (2006).
- [4] N. Loureiro, A. Schekochihin, and S. Cowley, Instability of current sheets and formation of plasmoid chains, *Phys. Plasmas* **14**, 100703 (2007).
- [5] W. Daughton, V. Roytershteyn, B.J. Albright, H. Karimabadi, L. Yin, and K.J. Bowers, Transition from Collisional to Kinetic Regimes in Large-Scale Reconnection Layers, *Phys. Rev. Lett.* **103**, 065004 (2009).
- [6] A. Bhattacharjee, Y.-M. Huang, H. Yang, and B. Rogers, Fast reconnection in high-Lundquist-number plasmas due to the plasmoid instability, *Phys. Plasmas* **16**, 112102 (2009).
- [7] H. Ji and W. Daughton, Phase diagram for magnetic reconnection in heliophysical, astrophysical, and laboratory plasmas, *Phys. Plasmas* **18**, 111207 (2011).
- [8] P. Sweet, The neutral point theory of solar flares, in *Electromagnetic Phenomena in Cosmical Physics*, edited by B. Lehnert (Cambridge University Press, Cambridge, England, 1958), p. 123.
- [9] E. N. Parker, Sweet's mechanism for merging magnetic fields in conducting fluids, *J. Geophys. Res.* **62**, 509 (1957).
- [10] D. Biskamp, Magnetic reconnection via current sheets, *Phys. Fluids* **29**, 1520 (1986).
- [11] H. Ji, M. Yamada, S. Hsu, and R. Kulsrud, Experimental Test of the Sweet-Parker Model of Magnetic Reconnection, *Phys. Rev. Lett.* **80**, 3256 (1998).
- [12] F. S. Mozer, S. D. Bale, and T. Phan, Evidence of Diffusion Regions at a Subsolar Magnetopause Crossing, *Phys. Rev. Lett.* **89**, 015002 (2002).
- [13] Y. Ren, M. Yamada, S. Gerhardt, H. Ji, R. Kulsrud, and A. Kuritsyn, Experimental Verification of the Hall Effect during Magnetic Reconnection in a Laboratory Plasma, *Phys. Rev. Lett.* **95**, 055003 (2005).
- [14] P. A. Cassak, M. A. Shay, and J. F. Drake, Catastrophe Model for Fast Magnetic Reconnection Onset, *Phys. Rev. Lett.* **95**, 235002 (2005).
- [15] M. Yamada, Y. Ren, H. Ji, J. Breslau, S. Gerhardt, R. Kulsrud, and A. Kuritsyn, Experimental study of two-fluid effects on magnetic reconnection in a laboratory plasma

- with variable collisionality, *Phys. Plasmas* **13**, 052119 (2006).
- [16] B. Ö. Sonnerup, Magnetic field reconnection, *Sol. Syst. Plasma Phys.* **3**, 45 (1979).
- [17] B. N. Rogers, R. E. Denton, J. F. Drake, and M. A. Shay, Role of Dispersive Waves in Collisionless Magnetic Reconnection, *Phys. Rev. Lett.* **87**, 195004 (2001).
- [18] M. Yamada, R. Kulsrud, and H. Ji, Magnetic reconnection, *Rev. Mod. Phys.* **82**, 603 (2010).
- [19] P. Cassak, M. Shay, and J. Drake, A saddle-node bifurcation model of magnetic reconnection onset, *Phys. Plasmas* **17**, 062105 (2010).
- [20] P. Cassak and J. Drake, On phase diagrams of magnetic reconnection, *Phys. Plasmas* **20**, 061207 (2013).
- [21] Y.-M. Huang, A. Bhattacharjee, and B. P. Sullivan, Onset of fast reconnection in hall magnetohydrodynamics mediated by the plasmoid instability, *Phys. Plasmas* **18**, 072109 (2011).
- [22] W. Daughton, V. Roytershteyn, B. Albright, H. Karimabadi, L. Yin, and K. J. Bowers, Influence of coulomb collisions on the structure of reconnection layers, *Phys. Plasmas* **16**, 072117 (2009).
- [23] W. Daughton, V. Roytershteyn, H. Karimabadi, L. Yin, B. Albright, S. Gary, and K. J. Bowers, Secondary Island formation in collisional and collisionless kinetic simulations of magnetic reconnection, *AIP Conf. Proc.* **1320**, 144 (2011).
- [24] A. Stanier, W. Daughton, A. Le, X. Li, and R. Bird, Influence of 3d plasmoid dynamics on the transition from collisional to kinetic reconnection, *Phys. Plasmas* **26**, 072121 (2019).
- [25] J. Jara-Almonte, H. Ji, J. Yoo, M. Yamada, W. Fox, and W. Daughton, Kinetic Simulations of Magnetic Reconnection in Partially Ionized Plasmas, *Phys. Rev. Lett.* **122**, 015101 (2019).
- [26] K. J. Bowers, B. Albright, L. Yin, B. Bergen, and T. Kwan, Ultrahigh performance three-dimensional electromagnetic relativistic kinetic plasma simulation, *Phys. Plasmas* **15**, 055703 (2008).
- [27] K. J. Bowers, B. J. Albright, L. Yin, W. Daughton, V. Roytershteyn, B. Bergen, and T. Kwan, Advances in petascale kinetic plasma simulation with VPIC and Roadrunner, *J. Phys. Conf. Ser.* **180**, 012055 (2009).
- [28] T. Takizuka and H. Abe, A binary collision model for plasma simulation with a particle code, *J. Comput. Phys.* **25**, 205 (1977).
- [29] J. Birn, M. Hesse, and K. Schindler, Entropy conservation in simulations of magnetic reconnection, *Phys. Plasmas* **13**, 092117 (2006).
- [30] H. Liang, P. A. Cassak, S. Servidio, M. A. Shay, J. F. Drake, M. Swisdak, M. R. Argall, J. C. Dorelli, E. E. Scime, W. H. Matthaeus *et al.*, Decomposition of plasma kinetic entropy into position and velocity space and the use of kinetic entropy in particle-in-cell simulations, *Phys. Plasmas* **26**, 082903 (2019).
- [31] S. Du, G. P. Zank, X. Li, and F. Guo, Energy dissipation and entropy in collisionless plasma, *Phys. Rev. E* **101**, 033208 (2020).
- [32] H. Liang, P. Cassak, M. Swisdak, and S. Servidio, Estimating effective collision frequency and kinetic entropy uncertainty in particle-in-cell simulations, *J. Phys. Conf. Ser.* **1620**, 012009 (2020).
- [33] P. Hall and S. C. Morton, On the estimation of entropy, *Ann. Inst. Stat. Math.* **45**, 69 (1993).
- [34] L. Kozachenko and N. N. Leonenko, Sample estimate of the entropy of a random vector, *Prob. Peredachi Inf.* **23**, 9 (1987).
- [35] T. B. Berrett, R. J. Samworth, M. Yuan, Efficient multivariate entropy estimation via  $k$ -nearest neighbour distances, *Ann. Stat.* **47**, 288 (2019).
- [36] See Supplemental Material at <http://link.aps.org/supplemental/10.1103/PhysRevLett.127.055102> for a discussion on  $E_{NG}$  and the KL estimator.
- [37] M. M. Kuznetsova, M. Hesse, and D. Winske, Kinetic quasi-viscous and bulk flow inertia effects in collisionless magnetotail reconnection, *J. Geophys. Res.* **103**, 199 (1998).
- [38] M. Hesse, K. Schindler, J. Birn, and M. Kuznetsova, The diffusion region in collisionless magnetic reconnection, *Phys. Plasmas* **6**, 1781 (1999).
- [39] S. I. Braginskii, Transport processes in a plasma, *Rev. Plasma Phys.* **1**, 205 (1965).
- [40] R. Schunk, Mathematical structure of transport equations for multispecies flows, *Rev. Geophys.* **15**, 429 (1977).
- [41] D. Biskamp, Instability of two-dimensional collisionless plasmas with neutral points, *Plasma Phys.* **13**, 1013 (1971).
- [42] J. Beirlant, E. J. Dudewicz, L. Györfi, and E. C. Van der Meulen, Nonparametric entropy estimation: An overview, *Int. J. Math. Stat. Sci.* **6**, 17 (1997).
- [43] J. Wygant, C. Cattell, R. Lysak, Y. Song, J. Dombeck, J. McFadden, F. Mozer, C. Carlson, G. Parks, E. Lucek *et al.*, Cluster observations of an intense normal component of the electric field at a thin reconnecting current sheet in the tail and its role in the shock-like acceleration of the ion fluid into the separatrix region, *J. Geophys. Research* **110**, A9 (2005).
- [44] W. Daughton and V. Roytershteyn, Emerging parameter space map of magnetic reconnection in collisional and kinetic regimes, *Space Sci. Rev.* **172**, 271 (2012).
- [45] A. Stanier, W. Daughton, L. Chacon, H. Karimabadi, J. Ng, Y.-M. Huang, A. Hakim, and A. Bhattacharjee, Role of Ion Kinetic Physics in the Interaction of Magnetic Flux Ropes, *Phys. Rev. Lett.* **115**, 175004 (2015).
- [46] J. Ng, Y.-M. Huang, A. Hakim, A. Bhattacharjee, A. Stanier, W. Daughton, L. Wang, and K. Germaschewski, The island coalescence problem: Scaling of reconnection in extended fluid models including higher-order moments, *Phys. Plasmas* **22**, 112104 (2015).
- [47] J. Jara-Almonte and H. Ji, Data for A thermodynamic phase transition in magnetic reconnection, Princeton University DataSpace, <http://arks.princeton.edu/ark:/88435/dsp018k71nm17d> (2021).